Chapter 5

Correlation holography with unpolarized light

In this chapter, we have presented two different correlation holography approaches with unpolarized light. Complete theoretical background and experimental configurations are described.

5.1 Introduction

The optical recording and numerical reconstruction of the complex field is a unique feature of digital holography (DH) (Hendry, 2006; Poon, 2006; Schnars, 2005; Yamaguchi, 2006). Digital holography (DH) has played a significant role in 3D displaying technology, medical diagnosis (Balasubramani, 2021; Shaked, 2012), non-destructive testing (Schnars, 2005), and quantitative phase imaging (Park, 2018). In DH, holograms are recorded by a digital detector such as CCD/CMOS and a recorded hologram is a numerical reconstruction for recovery of the complex optical signal. Here, complex optical signal refers to the amplitude and phase components of the light. The DH with different geometries have been developed, and significant among them are in-line, off-axis, and phase-shifting (Gabor, 1948; Leith, 1962; Yamaguchi, 2006). Off-axis holography is a common technique in which the reference beam is angularly tilted with respect to the object observation axis and is free from the twin image problem of in-line holography. Off-axis holography requires a carrier frequency while recording the hologram to avoid the overlapping of the image with the conjugate image alias (Leith, 1962; Gross, 2008). However, an off-axis holography geometry affects the reconstruction quality due to limited pixel size in the image sensors and sharing of the frequency space (Gross, 2008). Phase-shifting holography overcomes this issue by capturing several images with accurate different phase shifts between the consecutive images (Awatsuji, 2006; Micó, 2009; Nomura, 2007; Yamaguchi, 2006). However, these conventional holography reconstruction techniques are not useful for the recovery of the desired optical signal from random light.

Recently some significant attempts have been made on the DH with arbitrary coherence and with stochastic light such as optical scanning holography (OSH), Fresnel incoherent correlation holography (FINCH), and others (Liu, 2018; Ohta, 2022; Pedrini,

2012; Poon, 1996, 2006, 2014; Rosen; 2007, 2019; Tahara, 2017). OSH works on the principle of active optical heterodyne scanning. In OSH, a heterodyne interference fringe pattern is first generated without the information of the object, and the object target is then raster scanned via interference pattern (Liu, 2018). In the FINCH, a hologram is composed of the summation of the Fresnel zone plate (FZP) and recorded with incoherent light illumination using a single path and self-reference interferometer. An optical element (SLM, birefringent crystal, or double-focus lens) is introduced to generate two waves to record the incoherent hologram in the FINCH (Rosen, 2007). Recently polarization was combined with stochastic light to extract the polarization features of the object (Tahara, 2017). An imaging system with a low coherence illumination is also developed by combining microscopy with an off-axis holography geometry (Kolman, 2010).

Apart from these developments, another emerging area in holography with spatially random light has been investigated and is known as correlation holography (Takeda, 2005). Takeda and co-workers have significantly contributed to the design and development of various experimental configurations and applications of the CH (Naik, 2011, 2012, 2013; Takeda, 2005). The vCZ theorem and Hanbury Brown-Twiss (HBT) approach are two central results in the coherence optics and these two ideas are of paramount importance in the CH (Naik, 2011; Rosen, 2022; Takeda, 2005). The CH employs an analogy between the optical field and coherence function to reconstruct a holographically recorded object from the two-point complex correlation of the random field. Incoherent light is used to illuminate the coherently recorded hologram and to synthesize the statistical features of the light for 3D imaging (Naik, 2011; Takeda, 2005). The CH has opened new research avenues on recording and shaping the spatial coherence for spatial coherence tomography, imaging, profilometry (Duan, 2006; Dogariu, 2015

Naik, 2012, 2013; Takeda, 2010), and coherence current to name a few (Wang, W., 2006). Designing an appropriate interferometer to measure spatial coherence is an essential requirement for the recovery of signals in the CH. Recording of incoherent-object as complex spatial coherence using the Sagnac interferometer with a phase-shifting approach has been developed (Naik, 2013). In a recent development, the HBT approach was combined with off-axis holography to image the complex field in the correlation holography (Singh, R., 2014). The relation between the second and fourth-order Gaussian random field permits to use HBT approach in the CH and offers a novel insight into statistical optics to develop simple and stable un-conventional holography techniques (Chen, 2020; Singh, R., 2014; Soni, 2016; Vinu, 2020). Extension of the CH to the vectorial regime has also been demonstrated and some of these correlation holography techniques with polarization holograms are Stokes holography with second and fourth-order interferometers (Singh, R., 2012; Singh, D., 2018). These two vectorial holography techniques record information in the Stokes fringes and use incoherent illumination to reconstruct the polarimetric information. Recently, polarization fringes have also been used to develop phase-shifting coherence holography with the HBT approach (Chen, 2021) and in an enhanced field of view (Chen, 2022). All these techniques require the off-diagonal elements of the coherence-polarization (CP) matrix and an off-axis reference coherence wave is used to overcome the phase loss. The coherence and polarization features of the random light are characterized by the elements of the CP matrix (Wolf, 2007). The off-diagonal elements of the CP matrix are no longer preserved due to depolarization. Depolarization affects the imaging quality due to the incoherent coupling of light into unpolarized light (Janassek, 2018; Marco, 2021). Polarization filters are used in the case of depolarization and to enhance the contrast of the speckle patterns in conventional and correlation imaging (Chen, 2020, 2021, 2022; Singh, R., 2014; Soni,

2016; Vinu, 2016, 2019, 2020). Nevertheless, we report two new techniques for the reconstruction of the complex optical signal in the CH using illumination with un-polarized random light. Moreover, these techniques are free from the requirement of the angular separation between the coherence waves.

5.2 Stokes correlation of randomly polarized light

Consider a random orthogonally polarized light propagating along the z-axis. The orthogonal polarization components of the light are expressed as

$$E_H(r) = |E_H(r)|\exp[i\varphi_H(r)], \qquad E_V(r) = |E_V(r)|\exp[i\varphi_V(r)], \tag{5.1}$$

The subscripts *H* and *V* stand for horizontal and vertical polarization components and the coefficients $|E_H(r)|$ and $|E_V(r)|$ are the amplitude of the corresponding components with phases φ_H and φ_V respectively. The light field can be represented as a column matrix

$$E(r) = \begin{pmatrix} |E_H(r)|\exp[i\varphi_H(r)] \\ |E_V(r)|\exp[i\varphi_V(r)] \end{pmatrix}, \tag{5.2}$$

where *E(r)* represents the field at a particular instant of time t. The polarimetric information of the field can be estimated as

$$S_p(r) = E^{\dagger}(r)\sigma^p E(r), (p = 0, 1, 2, 3) \tag{5.3}$$

where † denotes the Hermitian conjugate. σ^0 denotes the 2 x 2 identity matrix, and the three Pauli spin matrices are defined as

$$\sigma^1 = \begin{pmatrix} 1 & 0 \\ 0 & -1 \end{pmatrix}, \sigma^2 = \begin{pmatrix} 0 & 1 \\ 1 & 0 \end{pmatrix}, \sigma^3 = \begin{pmatrix} 0 & -i \\ i & 0 \end{pmatrix}, \tag{5.4}$$

A fluctuation of the Stokes parameter with respect to its mean value is evaluated as

$$\Delta S_p(r) = S_p(r) - < S_p(r) >, \tag{5.5}$$

where $S_p(r)$ is the Stokes parameters at a particular spatial point and $<S_p(r)>$ denotes the mean value. The 4 × 4 SPs fluctuation correlation matrix $C_{pq}(r_1, r_2)$ is defined (Kuebel, 2019; Hannonen, 2020; Wu, 2019) as

$$C_{pq}(r_1, r_2) =< \Delta S_p(r_1)\Delta S_q(r_2) >, \quad (p, q=0, 1, 2, 3), \tag{5.6}$$

where r_1 and r_2 are two-position vectors at the observation plane and parenthesis <.> represents the ensemble average. A fourth-order correlation can be expressed in terms of the second-order correlation for the Gaussian random fields. Therefore, elements of the matrix are expressed (Kuebel, 2019; Wu, 2019) as

$$C_{pq}(r_1, r_2) = \sum_{k,l}\sum_{m,n} \sigma_{kl}^{p}\sigma_{mn}^{q} W_{kn}(r_1, r_2) W_{lm}^{*}(r_1, r_2), (k, l, m, n=x, y) \tag{5.7}$$

where $W_{kn}(r_1, r_2) =< E_k^{*}(r_1)E_n(r_2) >$ represent elements of the 2x2 coherence-polarization (CP) matrix. The off-diagonal elements of the CP matrix are null for unpolarized light and are represented (Kuebel, 2019) as

$$W(r_1, r_2) = \begin{pmatrix} W_{xx}(r_1, r_2) & 0 \\ 0 & W_{yy}(r_1, r_2) \end{pmatrix}, \tag{5.8}$$

Therefore, the 4x 4 matrix is transformed to

$$C_{pq}(r_1, r_2) = \begin{pmatrix} |W_{xx}|^2 + |W_{yy}|^2 & |W_{xx}|^2 - |W_{yy}|^2 & 0 & 0 \\ |W_{xx}|^2 - |W_{yy}|^2 & |W_{xx}|^2 + |W_{yy}|^2 & 0 & 0 \\ 0 & 0 & 2\,\mathrm{Re}[W_{xx}W_{yy}^{*}] & 2\,\mathrm{Im}[W_{xx}^{*}W_{yy}] \\ 0 & 0 & 2\,\mathrm{Im}[W_{xx}W_{yy}^{*}] & 2\,\mathrm{Re}[W_{xx}W_{yy}^{*}] \end{pmatrix}, \tag{5.9}$$

For brevity, the (r_1, r_2) dependence of the matrix elements is suppressed on the left-hand side in Eq. (5.9).

5.3 Higher-order Stokes correlation holography

The proposed technique utilizes the higher-order correlation of the SPs for the reconstruction of the hologram with random light and subsequent recovery of the complex-valued two-dimensional signal. This technique exploits a fundamental feature of the light and uses higher-order Stokes parameters (SPs) correlation of the random light to build a new reconstruction technique for the CH. This technique is free from the requirement of the angular separation between the interfering coherence waves and also offers a lensless Fourier transform connection between a desired two-point complex correlation at the observation plane with the incoherently illuminated hologram. Recently, SPs correlation was used to analyze random electromagnetic beams, and ghost polarimetry, (Hannonen, 2020; Wu, 2019). Inspired by the significance of the SPs in the characterization of the random fields, here we evolve a theoretical basis to develop a new holographic principle for the reconstruction of the hologram with random light where conventional holography reconstruction methods fail. The SPs of the random unpolarized light are used to extract SPs fluctuations correlations which imparts a 4 x 4 matrix with a total of sixteen elements. Out of these sixteen elements, only two elements of the matrix are utilized to develop a new reconstruction method for the CH. The proposed theoretical basis with experimental results validates a new reconstruction method for holography with random light. To the best of our knowledge, this is the first such attempt to build a holography technique without a carrier frequency in the 4^{th}-order correlation, and the technique offers holographic reconstruction without phase shifting, or iteration, and is also free from twin copies of the CH. A detailed theoretical basis, simulation, and experimental results are discussed below.

5.3.1 Theoretical basis

Two matrix elements $C_{22}(r_1, r_2)$, $C_{32}(r_1, r_2)$ are expressed as

$$C_{22}(r_1, r_2) = 2\,\mathrm{Re}[W_{xx}(r_1, r_2)W_{yy}^{*}(r_1, r_2)], \tag{5.10}$$

$$C_{32}(r_1, r_2) = 2\,\mathrm{Im}[W_{xx}(r_1, r_2)W_{yy}^{*}(r_1, r_2)], \tag{5.11}$$

Here, we introduce a new quantity called the complex polarization correlation function (CPCF) by adding Eq. (5.10) and (5.11) as

$$C(r_1, r_2) = C_{22}(r_1, r_2) + iC_{32}(r_1, r_2), \tag{5.12}$$

$$C(r_1, r_2) \propto \mathrm{Re}[W_{xx}(r_1, r_2)W_{yy}^{*}(r_1, r_2)] + i\,\mathrm{Im}[W_{xx}(r_1, r_2)W_{yy}^{*}(r_1, r_2)], \tag{5.13}$$

Now, we examine use of Eq. (5.13) in the reconstruction of an incoherent object illuminated with random unpolarized light. Here, the object is a Fourier transform hologram (FTH) (Lee, 1970) encoding the complex-valued information as shown in Fig. 5.1 (a). This hologram is illuminated with an incoherent light for the reconstruction as shown in Fig. 5.1(b). In order to use Eq. (5.13) in the CH and reconstruct the complex-valued object, a polarization component of the light illuminating the hologram is vertically polarized with desired coherence $W_{yy}(\Delta r)$. On the other hand, a horizontal polarization component is reserved for a reference coherence $W_{xx}(\Delta r)$.

The uniqueness of our strategy is also associated with independent control of two orthogonal polarization components, i.e. vertical for hologram illumination and horizontal for reference. A complex field represented in Eq. (5.2) is connected with the illuminating source as

$$E(r) = \int E(\hat{r}_1)G(r, \hat{r}_1)d\hat{r}_1, \tag{5.14}$$

$$E(r) = \frac{\exp(ikz)}{i\lambda z}\int \exp\left[\frac{ik}{2z}(|\,r\,|^2 - 2r.\hat{r}_1 + |\,\hat{r}_1\,|^2)\right]E(\hat{r}_1)d\hat{r}_1, \tag{5.15}$$

where $G(r,\hat{r}_j)=\dfrac{\exp(ikz)}{i\lambda z}\exp\left[\dfrac{ik}{2z}(r-\hat{r}_j)^2\right]$ is Fresnel kernel and other symbols have their usual meaning. A spatial position vector at the source plane is denoted by $\hat{r}_j$ ($j=1, 2$). Eq. (5.14) represents an instantaneous complex field and a member of the ensemble.

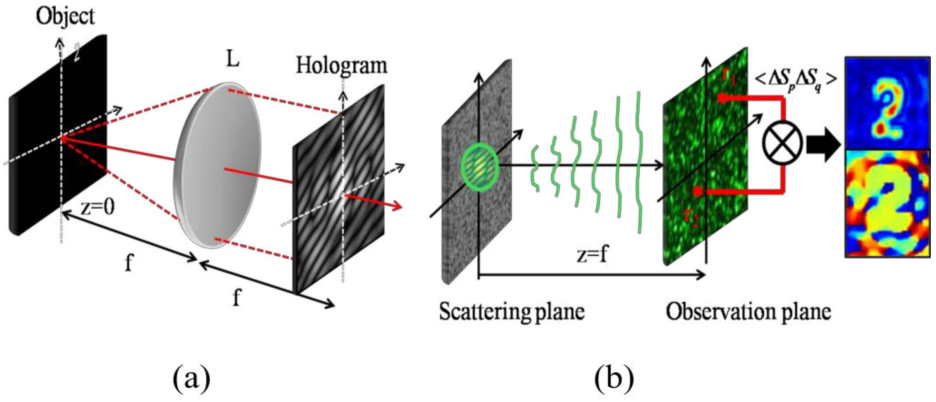

Fig. 5.1 Schematic representation of recoding and reconstruction of the FTH hologram. **(a)** denotes the recording of the FTH hologram, L represents the lens of focal length f. **(b)** shows the incoherent reconstruction of the FTH by random light at a distance $z=f$.

Substituting Eq. (5.14) into Eq. (5.12) helps to connect the CPCF with the elements of the CP matrix of the hologram and reference fields as follows

$$C(r_1,r_2)=W_{xx}^{R}(r_1,r_2)W_{yy}^{T*}(r_1,r_2)=<E_x^{R*}(r_1)E_x^{R}(r_2)><E_y^{T*}(r_1)E_y^{T}(r_2)>, \tag{5.16}$$

where T and R stand for transmittance of a hologram/or object and reference fields respectively.

Substituting Eq. (5.15) into Eq. (5.16) transforms the complex coherence function a

$$W_{pp}^{T}(r_1,r_2)=\frac{1}{\lambda^2 z^2}<A\int\int E_p^{*}(\hat{r}_1)E_P(\hat{r}_2)\exp\left(\frac{ik}{2z}[|\hat{r}_2|^2-|\hat{r}_1|^2]\right)\exp\left(\frac{-ik}{z}[r_2.\hat{r}_2-r_1.\hat{r}_1]\right)d\hat{r}_1 d\hat{r}_2>, \tag{5.17}$$

where p represents the orthogonal polarization component and T stands for transparency such as hologram or reference source. A phase term outside the integration is represented as $A = \exp\left(\frac{ik}{2z}|r_1|^2\right)\exp\left(-\frac{ik}{2z}|r_2|^2\right)$. A similar relation that exists for a reference source illuminated by a horizontally polarized light. Substitution of the complex fields in the Stokes correlation leads to the cancellation of a common phase curvature outside the integral and thus helps to achieve spatial stationarity at an arbitrary z plane. Spatial stationarity at the observation plane permits replacing the ensemble averaging with spatial averaging (Singh, R., 2013). Therefore, Eq. (5.17) modifies to

$$W_{pp}^{T}(\Delta r) \propto \int I_{pp}^{T}(\hat{r})\exp\left(-\frac{ik(\Delta r.\hat{r})}{z}\right)d\hat{r}, \tag{5.18}$$

where transmittance function for the hologram and reference are respectively $I_{yy}(\hat{r}) = |E_y(\hat{r})|^2$ and $I_{xx}(\hat{r}) = cir\left(\frac{\hat{r}}{a}\right)$, $a$represents aperture size at the scattering plane. The aperture size$a$is considered to be small in order to generate a uniform reference coherence $W_{xx}^{R}(\Delta r)$ to cover the support of $W_{yy}^{T*}(\Delta r)$ as desired in Eq. (5.16). Therefore Eq. (5.16) is represented as

$$W_{xx}^{R}(\Delta r)W_{yy}^{T*}(\Delta r) \propto \int I_{yy}(\hat{r})\exp\left(\frac{ik(\Delta r.\hat{r})}{z}\right)d\hat{r},$$

(5.19)

$I_{yy}(\hat{r})$ is a real function and represents the hologram. Eq. (5.19) is a vectorial vCZ theorem based on spatial averaging and this relation connects an incoherently/or randomly illuminated hologram with the complex coherence function at the z plane. Therefore, our strategy to independently deal with the orthogonal polarization components and use random polarization in the higher-order Stokes parameters

correlation helps to achieve a lensless Fourier transform with the coherence waves and hence reconstruct the FTH hologram by a single Fourier transform.

5.3.2 Simulation results

To illustrate the validation of our approach, we simulate an experimental situation wherein a hologram is illuminated by the random field as represented in Fig. 5.1(b). An object located at an off-axis position as represented in Fig. 5.1 (a) is encoded into the FTH (Lee, 1970). Conventional reconstruction of the FTH is not possible with random field illumination. We have simulated the Fourier hologram for two different objects, namely a vortex and a number 2 with $f=250$ mm. A vortex is a phase object with a topological charge $l=1$ where the topological charge represents a phase variation of 2π around the singularity (Torres, 2011). Simulation is realized for orthogonally polarized random light fields with wavelength $\lambda = 532$ nm. The random fields for two orthogonal polarization components are modeled by considering two different and independent phase screens with phase variation with equal probability distribution in the range of $[-\pi, \pi]$. A random field coming out of the hologram is considered to be vertically polarized and propagation from the source to the observation plane at z=250 mm is modeled using a Fresnel propagation kernel. Similarly, a horizontally polarized light emerging out of the reference phase screen propagation to the observation plane located at z=250 mm is modeled using the Fresnel propagation kernel. A reference random field is generated by a circular aperture source of size $a = 0.8$ mm whereas the hologram size is 5 mm. Therefore, a random field at the observation plane is comprised of contributions from two independent and orthogonally polarized random sources, i.e. one from the hologram and the second from the reference. The Stokes parameters of the random field at the observation plane z=250 mm are obtained from the digitally propagated coherent random fields. These simulated Stokes parameters are used to extract the higher-order Stokes

fluctuations correlations as explained in Eq. (5.16) and utilized to reconstruct the hologram. The higher-order Stokes fluctuation correlations $C_{22}(\Delta r)$, $C_{32}(\Delta r)$ are obtained by using spatial averaging as follows.

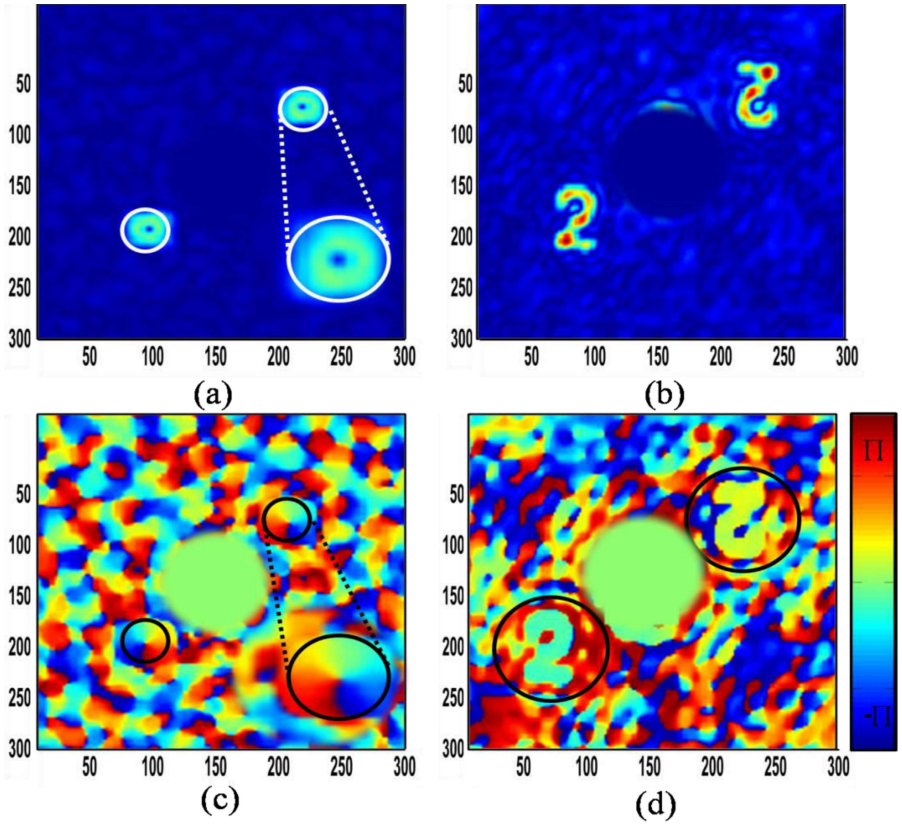

Fig. 5.2 Simulation results: **(a, b)** represent amplitude distribution of the vortex with *l=1* and number 2. **(c, d)** are the corresponding phase distribution. The magnified images of the amplitude and phase distribution of the vortex are shown in the inset of Figs. 5.2 **(a)** and 5.2 **(c)** respectively. Pixel numbers are given on both axes.

Spatial averaging is implemented by taking a portion of the desired Stokes parameters of the speckle pattern at the observation plane as a matrix $S_n^m(x, y)$ where n=2, 3, and m represents a particular realization of the random field. Here x and y are pixel spatial coordinates and take values up to 300x300 pixels. The Stokes fluctuation correlation is obtained by correlating $\Delta S_n^m(x, y)\Delta S_n^m(0,0)$ for the deferent realization of the window of the speckle pattern and this process is represented as $\sum_{m=1}^{M}[\Delta S_n^m(x, y)\Delta S_n^m(0,0)]/M$. Here M

represents the number of different realizations of the matrix $S_n^m(x,y)$ and produced by the pixel-by-pixel movement of the matrix $S_n^m(x,y)$ over the speckle pattern. We have considered the window of size (x,y) =300x300 pixels and 2D scanning of $S_n^m(x,y)$ over the speckle pattern provides 700x700 different realizations in the spatial averaging. Out of the simulated SPs, only S_2, and S_3 are used to reconstruct the hologram as discussed in Eq. (5.20). The simulated reconstruction for two different holograms, namely with vortex and number 2 is shown in Fig. 5.2 using the Stokes fluctuation correlations. Figs 5.2, (a), and (b) represent the amplitude distribution of the vortex and number 2 and Figs. 5.2, (c), and (d) show corresponding phase distributions.

5.3.3 Experiment and results discussions

Validation of the proposed technique is also confirmed by an experimental system designed in a collinear geometry as shown in Fig. 5.3. A spatially filtered collimated unpolarized diode laser light with a wavelength of 532 nm beam propagates through a polarization beam splitter (PBS) and subsequently, the beam divides into two orthogonal polarization components i.e horizontal and vertical. The PBS is used in the beginning to generate two independently orthogonally polarized random fields as follows. A vertical polarization component reflected by the PBS illuminates the spatial light modulator (SLM) through a beam splitter (BS1). A beam reflected by the BS1, in the beginning, is dumped and not used in the experiment as represented by the beam dumper. A computer-generated hologram is displayed on the SLM (Holoeye LC-R 720) and loaded into reflected light from the SLM. This SLM is different from previously used SLM in chapters 2 and 3. This reflected beam is further guided by the BS1 toward a ground glass GG1 and propagates toward the CCD. A linear polarizer (LP1) is placed after the BS1 to filter the vertical polarization component of the beam coming from the SLM. The distance between the hologram and the ground glass is considered to be negligible. The

information encoded into the hologram is spatially scrambled by the diffuser GG1 and the speckle pattern of the vertically polarized light is produced at the observation plane without any direct resemblance to the object encoded into the FTH.

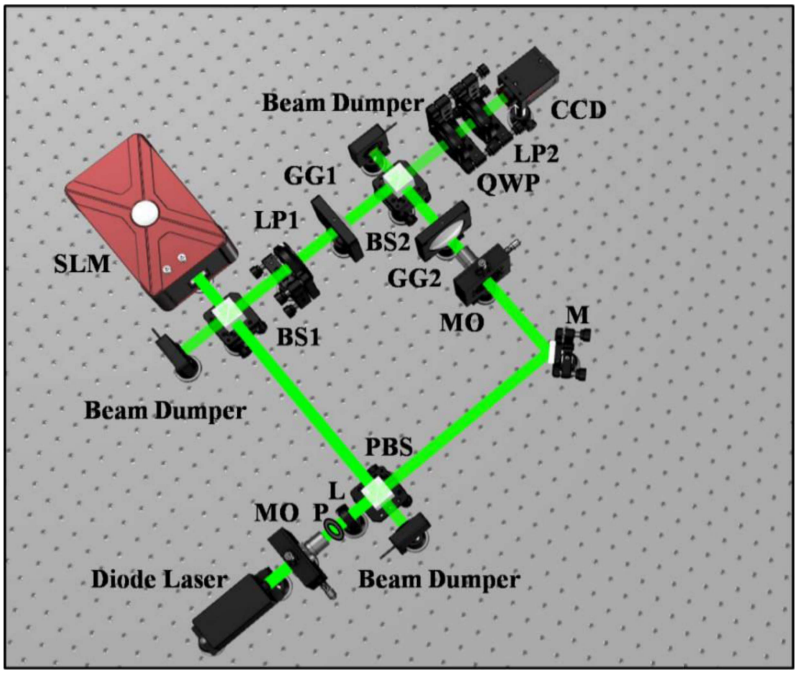

Fig. 5.3 Experimental implementation of the proposed technique. Laser: Solid random polarized diode laser, MO: Microscope objectives, P: Pinhole, L: lens, PBS: Polarizing beam splitter, M: Mirror, SLM: Spatial light modulator, GG1, GG2: Ground glasses, BS1, BS2: Beam splitters, QWP: Quarter wave plate, LP1, LP2: Linear polarizers, CCD: Charge-coupled device.

On the other hand, a transmitted horizontal polarization component from the PBS is folded by a mirror M and then focused by a microscope objective (MO-10 X) at the ground glass diffuser GG2 to generate a reference random field. The random field coming out of the GG2 is independent of the speckle of GG1 and this justifies consideration of no correlation of the orthogonal random fields at the observation plane, i.e. $< E_k^*(\hat{r}_1)E_l(\hat{r}_2) >= 0$. In order to measure the spatially varying SPs and characterize the random field at the observation plane, we inserted a quarter-waveplate and linear polarizer (LP2) before the charged-coupled device (CCD). The SPs of the random light are measured by rotating the

QWP at an angle θ_q to the x-direction and filtering by an LP. The transmission axis of the LP is set in the x-direction to the QWP and the resultant field is recorded by the CCD which has a resolution of 2200 x 2750 pixels, a dynamic range of 8 bits, and a pixel pitch of 4.54 μm [Procilica, GT 2750]. The CCD is placed at a distance of z= 250 mm from the diffusers and this distance is the same as the focal length of digital lens *f* in the FTH as in Fig. 5.1(a). The two SPs are evaluated from the captured speckle pattern using the following equation (Goldstein, 2017).

$$S_2(r) = I(45^0, 45^0) - I(135^0, 135^0), \tag{5.20}$$

$$S_3(r) = I(0^0, 45^0) - I(0^0, 135^0), \tag{5.21}$$

where $I(\theta_q, \theta_p)$ represent the intensity at the observation plane. θ_q, θ_p denote the orientation of the optic axis of QWP and LP with respect to the horizontal direction.

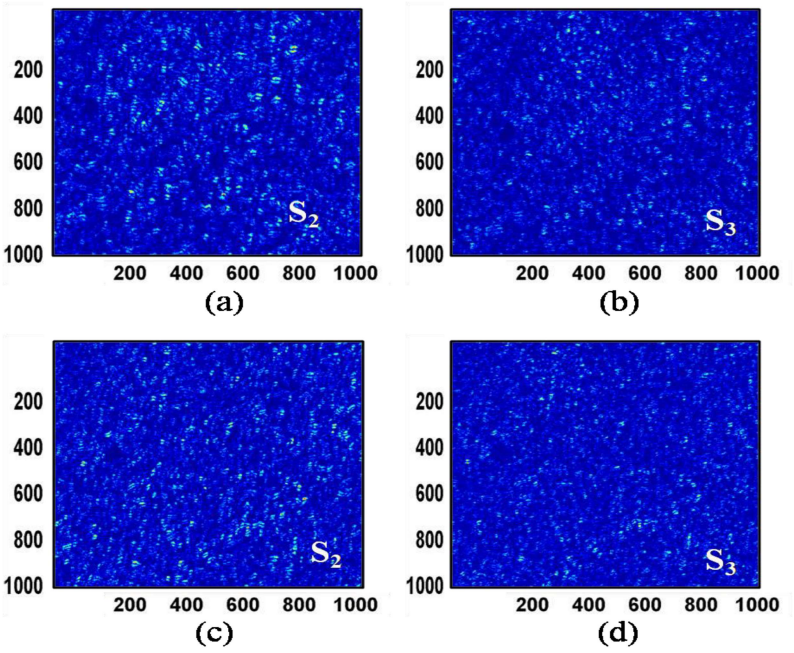

Fig. 5.4 Represent experimentally measured SPs from the captured intensity patterns. **(a,b)** represent SPs of the vortex with *l=1* and **(c, d)** show SPs of number 2. Pixel numbers are given on both axes.

The correlation between SPs fluctuations is evaluated from the experimentally measured SPs as in Eq. (5.6) and using spatial averaging as a replacement for ensemble averaging. This process provides the CPCF from the experimental measured SPs as explained in Eq. (5.13). Finally, the recovered CPCF is used to reconstruct the complex amplitude encoded into the hologram. To experimentally test the proposed technique, we have taken two different holograms with a vortex and number 2 as explained in the simulation. Experimentally measured desired SPs from the intensity speckle pattern for vortex and number 2 are shown in Fig. 5.4. The reconstructed amplitude and phase of the vortex with $l=1$ from the random light are shown in Fig. 5.5, (a) and (b). Likewise, the reconstructed amplitude and phase of the number 2 are shown in Fig 5.5 (c) and (d).

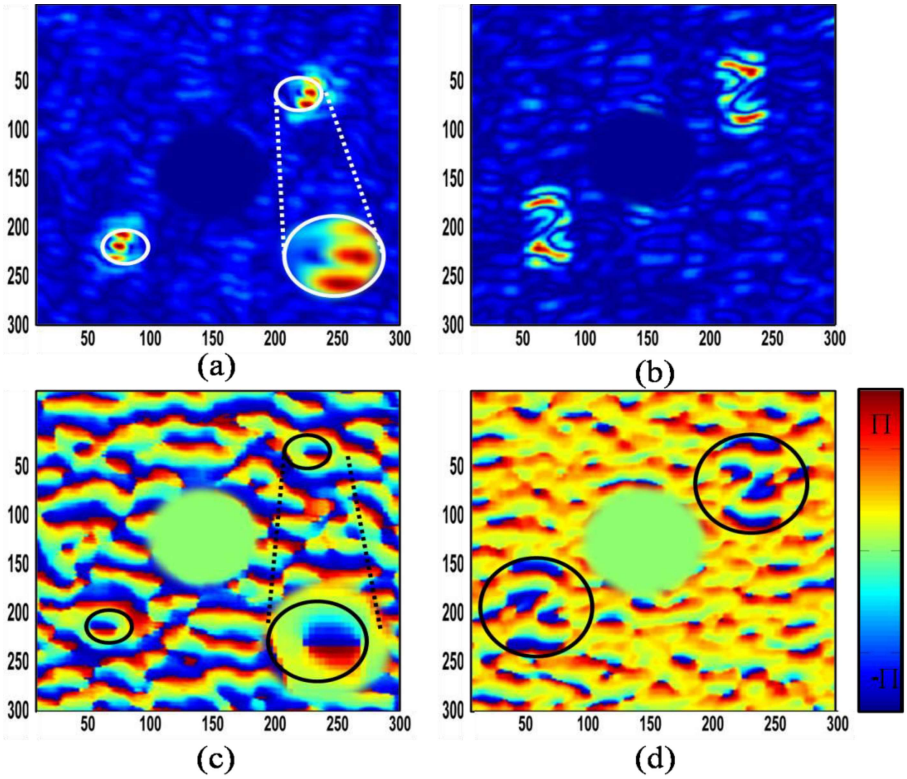

Fig. 5.5 Experimental results: **(a, b)** represent amplitude distribution of the vortex with $l=1$ and number 2. **(c, d)** are the corresponding phase distribution. The magnified images of the amplitude and phase distribution of the vortex are shown in the inset of Figs. 5.5**(a)** and 5.5**(c)** respectively. Pixel numbers are given on both axes.

The cross-covariance of the experimentally recorded SPs (S_2, S_3) is evaluated by considering spatial averaging under the condition of spatial ergodicity at the observation plane (rather than in time). The mileages of spatial averaging have been utilized recently in several correlation imaging approaches with due importance in spatial statistical optics [Takeda, 2014]. In order to highlight the reconstruction of an off-axis hologram and highlight the reconstructed object, a central DC term is digitally suppressed as shown in Fig. 5.5. The imaging quality of the proposed technique depends on the realization of the spatial stationarity of the random field at the CCD plane, the size of the polarization optics, and the incident source. The reconstruction quality is affected by the strength of the unpolarized source (Kellock, 2012), and any leakage in the orthogonal polarization components due to optical elements will affect reconstruction quality. The reconstruction quality of the hologram is also affected owing to the short coherence length of the used random polarized diode laser in the experiment which brings coherent noise in the reconstructed phase (Lee, Y., 2013).

5.4 On-axis phase-shifting correlation holography

Our goal in this technique is to use and exploit the randomness of the polarization for recovery of the complex coherence in correlation holography. The randomness of the polarization has been used to design and develop some unconventional imaging methods based on Ghost imaging or polarimetry (Chirkin, 2018; Janassek, 2018; Shi, 2014). Here, we propose and develop a new on-axis phase-shifting technique for the reconstruction of a hologram with un-polarized light which helps to realize a compact and highly stable experimental geometry for the correlation holography. Our technique is implemented by obtaining the correlation between Stokes parameters (SPs) fluctuations of the random field and using randomness in polarization along with four-step phase-shifting. The Stokes parameters (SPs) fluctuations correlation is extracted from the SP (S_2) of the

random light and used to retrieve the complex polarization cross-covariance (CPCF), subsequently, this supports recovery of phase in the correlation holography and hence reconstructs the complex-valued object encoded into the digital hologram. The proposed theoretical basis is verified by simulation results and experimental tests. The detailed theoretical basis, simulation, and experimental results are discussed below.

5.4.1 Theoretical background

Let us consider the correlation between the same Stokes fluctuations (ΔS_2) of the un-polarized field is evaluated using Eq. (5.7) as

$$C_{\mathrm{Re}}(r_1, r_2) = \langle \Delta S_2(r_1) \Delta S_2(r_2) \rangle = 2\,\mathrm{Re}\left[\left\langle E_x^*(r_1) E_x(r_2) \right\rangle \left\langle \left\{ E_y^*(r_1) E_y(r_2) \right\}^* \right\rangle \right], \tag{5.22}$$

Eq. (5.22) uses the correlation of only one Stokes parameter S_2 to retrieve the real part of the CPCF. Therefore, consideration of depolarization in the randomly scattered light field helps to build a new theoretical basis for a reconstruction of the incoherently illuminated hologram from the Stokes parameter S_2 in a lensless geometry as shown in Fig. 5.6.

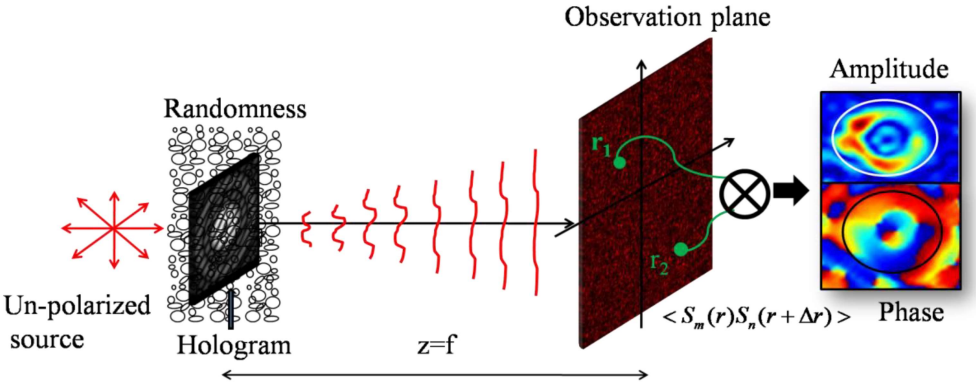

Fig. 5.6 Schematic representation: Reconstruction of the FH with un-polarized light from the randomness.

Consider that the y-polarization state of the light is loaded with a hologram displayed at the scattering plane, and the x-polarization state is reserved as a reference field. The

coherence function of the randomly scattered light field at any arbitrary distance z is connected to the source as

$$\left\langle E_i^*(r_1)E_j(r_2)\right\rangle = \int\int G^*(r_1,\hat{r}_1)G(r_2,\hat{r}_2)\left\langle E_i^*(\hat{r}_1)E_j(\hat{r}_2)\right\rangle d\hat{r}_1 d\hat{r}_2, \quad (i,j=x,y), \tag{5.23}$$

where $E(\hat{r})$ represents the source field and $\hat{r}$ indicates the spatial position vector at the source plane, and $G(r,\hat{r}_j) = \frac{-ik}{2\pi z}\exp\left[\frac{ik}{2}\left\{\frac{(r-\hat{r}_j)^2}{z}\right\}\right]$, $j=1,\ 2$, where $k = 2\pi/\lambda$ denotes wavenumber and λ represents a wavelength of the light. The constant phase term associated with the Fresnel kernel is ignored for a common z-plane. The ensemble averaging in Eq. (5.23) is supplanted by spatial averaging by assuming that the light field is stationary and ergodic in space which helps to develop a lensless imaging system. This spatial averaging condition is obtained by passing light through the static diffuser in the experiment. One can also replace ensemble averaging with time averaging by considering a rotating diffuser. Here, we rewrite the coherence function in Eq. (5.23) in terms of spatial averaging and consider $r_2 = r_1 + \Delta r$ (Singh, R., 2013). Therefore coherence function in Eq. (5.23) modifies as

$$\left\langle E_y^*(r)E_y(r+\Delta r)\right\rangle = \int H_{yy}(\hat{r})\exp\left[\frac{-ik}{z}\Delta r.\hat{r}\right]d\hat{r}, \tag{5.24}$$

$$\left\langle E_x^*(r)E_x(r+\Delta r)\right\rangle = \int I_{xx}(\hat{r})\exp\left[\frac{-ik}{z}\Delta r.\hat{r}\right]d\hat{r}, \tag{5.25}$$

Now y-polarization state is loaded with a hologram, $E_y(\hat{r}) = \left\{|H_y(\hat{r})|\exp[i\varphi_y(\hat{r})]\right\}\exp(i\delta(\hat{r}))$, $|H_y(\hat{r})|$ is the amplitude of the hologram, $\varphi_y(\hat{r})$ represent the deterministic phase of the read-out light, and $\delta(\hat{r})$ is the random phase

introduced to destroy spatial coherence by making light pass through a static diffuser in the proposed experiment.

$$\left\langle E_y^*(r)E_y(r+\Delta r)\right\rangle = \int H_{yy}(\hat{r})\exp\left[\frac{-ik}{z}\Delta r.\hat{r}\right]d\hat{r}, \tag{5.26}$$

$$\text{and}\left\langle E_x^*(r)E_x(r+\Delta r)\right\rangle = \int I_{xx}(\hat{r})\exp\left[\frac{-ik}{z}\Delta r.\hat{r}\right]d\hat{r}, \tag{5.27}$$

Eq. (5.27) & (5.28) are the vCZ theorem that connects the source at the diffuser plane with the far-field complex coherence function. Substituting Eq. (5.26) & Eq. (5.27) into Eq. (5.23), therefore, Eq. (5.23) transforms as

$$C_{\text{Re}}(\Delta r) \propto \text{Re}\left[\left\{FT\left\{H_{yy}(\hat{r})\right\}\right\}^* FT\left\{I_{xx}(\hat{r})\right\}\right], \tag{5.28}$$

where $H_{yy}(\hat{r}) = \left|O_y^{\varphi}(\hat{r}) + R(\hat{r})\right|^2$ denotes the digital hologram displayed at the scattering plane as shown in Fig. 5.6 and $I_{xx}(\hat{r}) = cir(\hat{r}/a)$ is the on-axis reference source of size a at the scattering plane. $\hat{r}$ is the spatial position vector at the source plane. Randomness introduced in the path of light due to scatterer and un-polarized light is washed out in the correlation measurement as described by Eq. (5.23). A phase shift φ is digitally introduced into the object beam $O_y^{\varphi}(\hat{r})$ encoded into the hologram $H_{yy}(\hat{r})$. A reference $R(\hat{r})$ encodes the complex-valued object $O_y^{\varphi}(\hat{r})$ into the hologram. Eq. (5.28) is combined with the four-step phase-shifting formula to retrieve the CPCF (Mandal, 2022) as follows

$$C(\Delta r) = [C_{\text{Re}}^0(\Delta r) - C_{\text{Re}}^{\pi}(\Delta r)] + i\,[C_{\text{Re}}^{\pi/2}(\Delta r) - C_{\text{Re}}^{3\pi/2}(\Delta r)], \tag{5.29}$$

where $C_{\text{Re}}^0(\Delta r)$, $C_{\text{Re}}^{\pi/2}(\Delta r)$, $C_{\text{Re}}^{\pi}(\Delta r)$, and $C_{\text{Re}}^{3\pi/2}(\Delta r)$ represent the real part of the CPCF with phase shifts of $0, \pi/2, \pi$ and $3\pi/2$ respectively. The CPCF renders the object information and helps to extract the complex amplitude of the object.

5.4.2 Simulation results

To validate the proposed technique, we have simulated the Fourier hologram for three different objects, namely a vortex beam with TC *l=1, 3,* and a Laguerre Gaussian beam with *l=1*, and *p=1* with *f=186* mm. A vortex is a phase object with a topological charge *l=1* where the TC represents a phase variation of 2π around the singularity (Torres, 2011). Simulation is implemented for orthogonally polarized random light fields with wavelength $\lambda = 632.8$ nm. The two different and independent phase screens with phase variation with equal probability distribution in the range of $[-\pi, \pi]$ are considered to model two random fields for the orthogonal polarization states. A random field coming out of the hologram is considered to be vertically polarized and propagation from the source to the observation plane at z=186 mm is modeled using a Fresnel propagation kernel. Similarly, a horizontally polarized light emerging out of the reference phase screen propagates to the observation plane located at z=186 mm using the Fresnel propagation kernel. A reference random field is generated by a circular aperture source of size $a = 0.8$ mm whereas the hologram size is 5 mm. Therefore, a random field at the observation plane is comprised of contributions from two independent and orthogonally polarized random sources, i.e. one from the hologram and the second from the reference. The Stokes parameters of the random field at the observation plane z=186 mm are obtained from the digitally propagated coherent random fields. These simulated Stokes parameters are used to extract the higher-order Stokes fluctuations correlations as explained in Eq. (5.22) and utilized to reconstruct the hologram. The higher-order Stokes fluctuation correlation $C_{22}(\Delta r)$ is evaluated by using spatial averaging as explained in section 5.1.2. Using Eq. (5.29), the reconstructed complex fields are shown in Fig. 5.7 for simulation. The amplitude distributions of the CPCF for the helical phase with *TC l=1, 3* are shown in Figs. 5.7, (a) & (b). Corresponding phase distributions are represented in

Figs. 5.7, (d) & (e) respectively. Figs. 5.7, (c) & (f) show amplitude and phase distribution of CPCF for Laguerre-Gaussian mode with *l=1, p=1*.

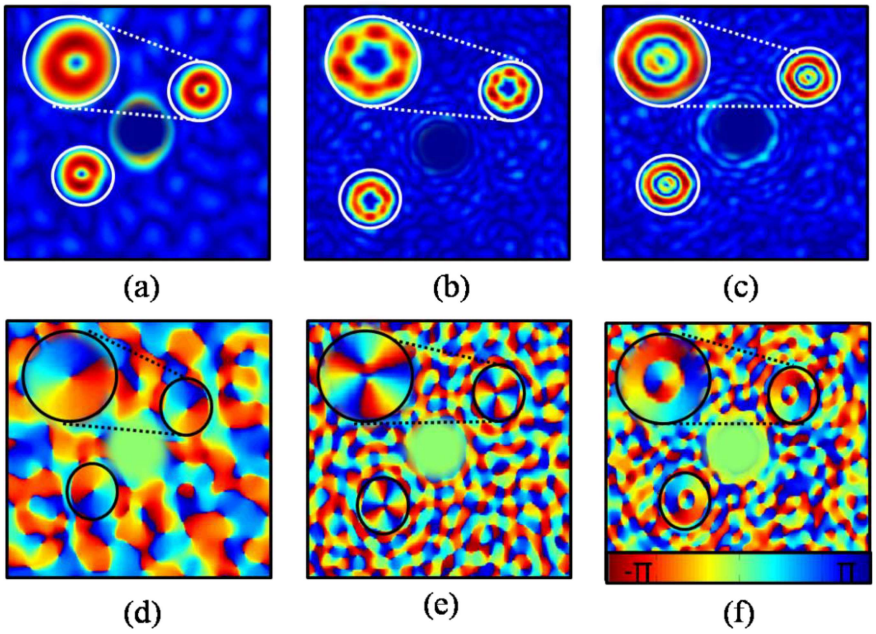

Fig. 5.7 (a, b) show the amplitude distribution of the vortex beam with TC *l=1, 3,* and **(d, e)** are the corresponding phase profile respectively. **(c)** indicates the amplitude profile of the Laguerre-Gaussian beam with mode *l=1, p=1*, **(f)** denotes the corresponding phase profile respectively.

5.4.3 Experiment and results discussions

To experimentally demonstrate the proposed method we designed a highly compact and stable in-line experimental geometry for the phase-shifting correlation holography with un-polarized light as shown in Fig. 5.8. A detailed description of the experimental method is as follows. An un-polarized He-Ne laser (HNL100RB, Thorlabs) light with wavelength 632.8 nm is spatially filtered by a spatial filter assembly composed of microscopic objective and pinhole. The lens (L_1) with a focal length of 200 mm is used to collimate the spatially filtered beam. The collimated beam is passed through the polarization beam splitter (PBS) which divides the beam into two orthogonal polarization components i.e horizontal and vertical. The half-wave plates (HWP_1 and HWP_2) are used to orient the

incident polarization states. The vertical polarization component, called the object beam illuminates the SLM (Holoeye LCR-720) with a pixel pitch of 20 μm on which off-axis Fourier transform hologram (FTH) with different phase shifts are displayed. The horizontal polarization component is reflected by the mirror (M). The strengths of both orthogonal polarization components, one from the SLM and the other from a mirror, are maintained to keep the un-polarized nature of the light intact. Now, these two orthogonal polarization components propagate through the PBS and further travel toward the lens L_3. Lens L_3 focuses the light, coming from mirror M, at the ground glass (GG) as shown in the inset in Fig. 2 by blue color.

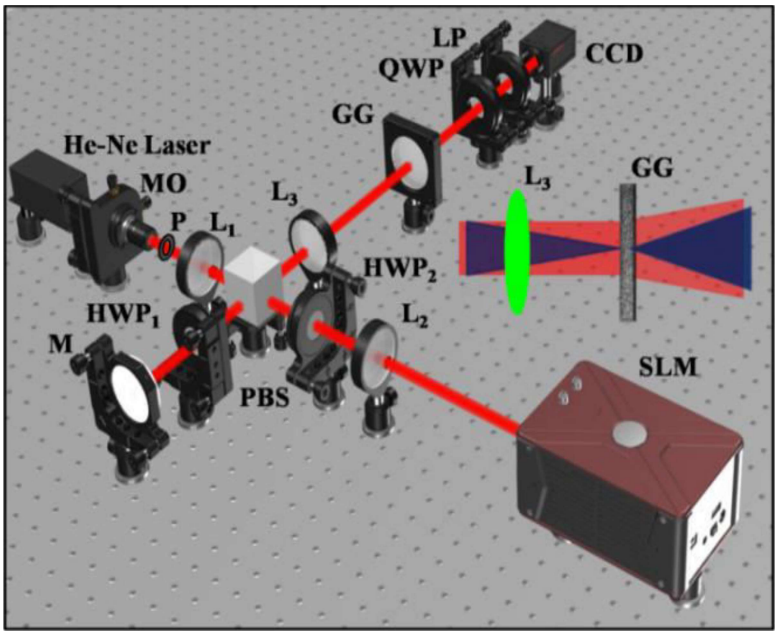

Fig. 5.8 Schematic of the optical set-up. He-Ne Laser, MO: microscopic objective, P: pinhole, L_1, L_2, L_3: lenses, PBS: polarizing beam splitter, HWP_1, HWP_2: half-wave plates, M: mirror, SLM: spatial light modulator, GG ground glass, QWP: quarter-wave plate, LP: linear polarizer, CCD: charge-coupled device. The propagation of the object beam (red) and reference beam (blue) from L_3 to GG is shown in the inset.

On one hand, lens combinations L_2 and L_3 are used to image light from the SLM plane to the GG plane as shown by the red color in the inset. To increase the size of the illumination beam, the SLM is placed slightly moved away from the focal plane (150

mm) of the lens L2 and the size of the illumination beam at the SLM is fixed around 5 mm. On the other hand, the reflected beam from the mirror is focused at an on-axis position on the GG using lens L_3. The GG randomly scatters the light field and generates a speckle pattern at the observation plane. Since the incident light source is un-polarized therefore correlation of the orthogonal polarization components of the random field at the detector is $\left\langle E_x^*(r_1)E_y(r_1+\Delta r\right\rangle = 0.$ Now, the quarter-wave plate and linear polarizer (LP) are inserted to measure the SP at the detector plane. A desired SP of the random light is measured by rotating the QWP at an angle θ_q with respect to the x-direction and filtering by an LP. The transmission axis of the LP is set in the x-direction with respect to the QWP and the resultant field is recorded by the Charge-coupled device (CCD) which has a resolution of 2200 x 2752 pixels, a dynamic range of 8 bit, and pixel pitch of 4.54 μm [Procilica, GT 2750]. The CCD camera is placed at a distance of z=186 mm from the scattering media, and in a lensless condition. The desired SP is evaluated from the captured intensity patterns using the following equation (Goldstein, 2017)

$$S_2(r) = I(45^0,45^0) - I(135^0,135^0), \tag{5.30}$$

where $I(\theta_q,\theta_p)$ represent the intensity at the observation plane. θ_q,θ_p denote the orientation of the optic axis of QWP and LP with respect to the horizontal direction.

The correlation between SP fluctuations is evaluated from the experimentally measured SP as explained in the theoretical basis and subsequently, the real part of the CPCF is measured using Eq. (5.23). Finally, the complex field of the object is retrieved by using Eq. (5.29). To validate the proposed technique, we have examined the reconstruction of the FTH displayed by the SLM.

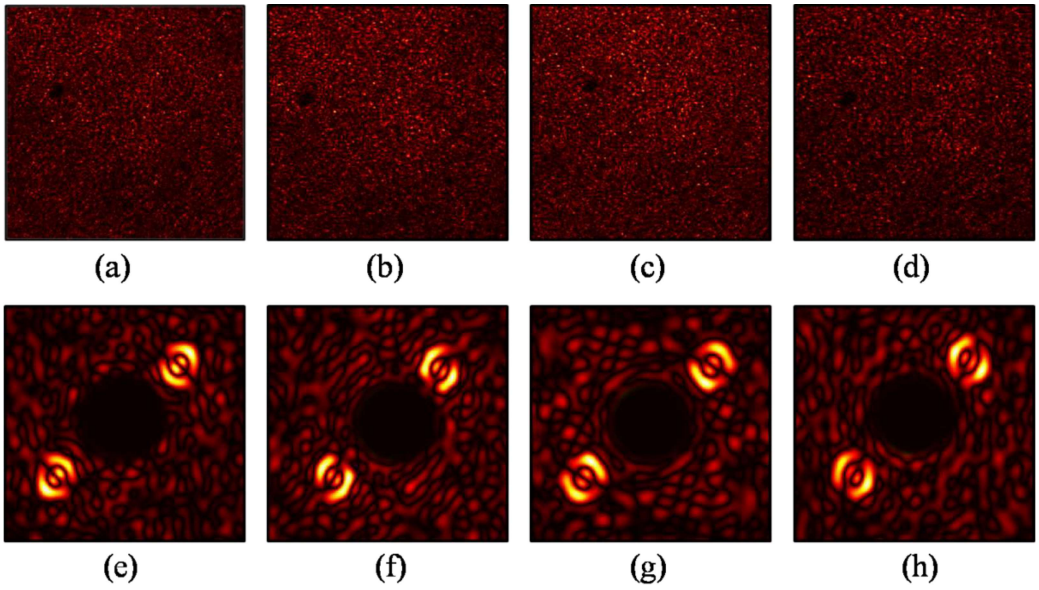

Fig. 5.9 (a-d) Represent experimentally measured S_2 for phase shifts of 0, $\pi/2$, π, and $3\pi/2$ of the Laguerre-Gaussian mode with *l=1, p=1*. **(e-h)** are the corresponding real part of the CPCF.

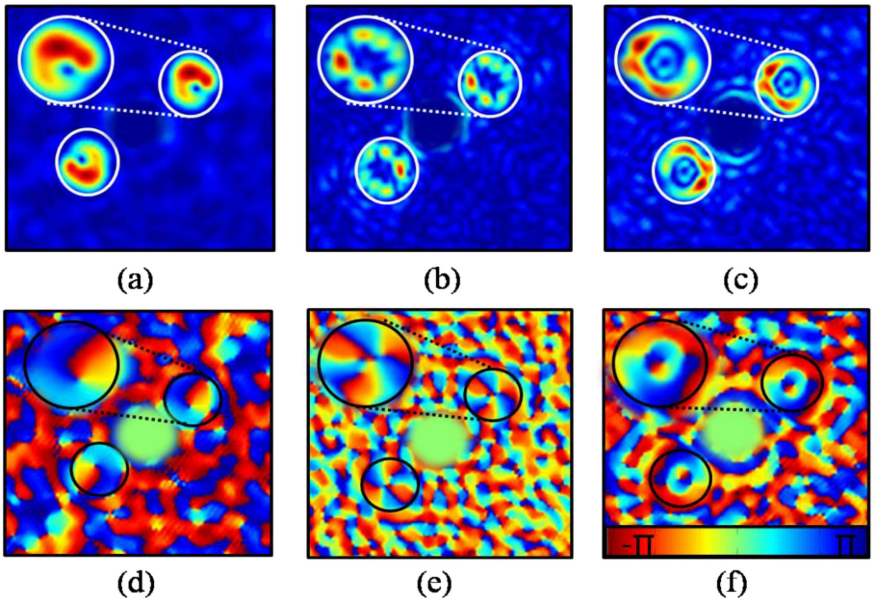

Fig. 5.10 (a, b) show the amplitude distribution of the vortex beam with TC *l=1, 3,* **(d, e)** are the corresponding phase profile respectively. **(c)** indicates the amplitude profile of the Laguerre-Gaussian beam with mode *l=1, p=1*, and **(f)** denotes the corresponding phase profile respectively.

Here, we consider an off-axis FTH $H_{yy}(\hat{r})$ encoding pure phase samples namely, vortex phases with topological charges (TC) *l=1, 3* and the Laguerre Gaussian beam with

azimuthal mode *l=1* and radial mode *p=1*. The TC represents phase variation around the center in the order of $l\ (2\pi)$. The experimentally measured SPs (S_2) for different phase shifts of $0, \pi/2, \pi,$ and $3\pi/2$ for the Laguerre-Gaussian mode with TC *l=1, p=1* are represented in Fig. 5.9. Figs. 5.9, (e-h) indicate the real part $C_{\mathrm{Re}}^{0}(\Delta r)$, $C_{\mathrm{Re}}^{\pi/2}(\Delta r)$, $C_{\mathrm{Re}}^{\pi}(\Delta r)$, and $C_{\mathrm{Re}}^{3\pi/2}(\Delta r)$ of the CPCF with phase shifts of $0, \pi/2, \pi,$ and $3\pi/2$.

The reconstructed complex fields are shown in Fig. 5.10 for the experiment. The amplitude distributions of the CPCF for the helical phase with *TC l=1, 3* are shown in Figs. 5.10, (a) & (b). Corresponding phase distributions are represented in Figs. 5.10, (d) & (e) respectively. Figs. 5.10, (c) & (f) show amplitude and phase distribution of CPCF for Laguerre-Gaussian mode with *l=1, p=1*. The cross-covariance of the experimentally recorded SP (S_2) is evaluated by applying spatial averaging at the detector plane under the condition of spatial ergodicity (rather than in time) as explained earlier. The imaging quality of the proposed technique depends on the realization of the spatial stationarity of the random field at the CCD plane and limited-size polarization optics.

5.5 Conclusion

In this chapter, we have proposed and experimentally demonstrated novel on-axis coherence holography techniques with unpolarized light. These techniques utilize depolarization of the orthogonal polarization components along with correlation of the Stokes parameter for the reconstruction of the hologram from the randomly scattered light. The proposed experimental technique is compact and highly stable which offers flexibility and robustness owing to in-line geometry in the correlation measurement. We have further verified the applicability of the proposed technique by recovering the complex field of the different objects from the random light. The proposed technique is

expected to find applications in imaging in the presence of depolarization mechanism, and coherence analysis.